

Magnetic helicity fluxes in an α^2 dynamo embedded in a halo

Alexander Hubbard† and Axel Brandenburg†‡

†NORDITA, AlbaNova University Center, Roslagstullsbacken 23, SE 10691 Stockholm, Sweden

‡Department of Astronomy, Stockholm University, SE 10691 Stockholm, Sweden

(Received 00 Month 200x; in final form 00 Month 200x)

We present the results of simulations of forced turbulence in a slab where the mean kinetic helicity has a maximum near the mid-plane, generating gradients of magnetic helicity of both large and small-scale fields. We also study systems that have poorly conducting buffer zones away from the midplane in order to assess the effects of boundaries. The dynamical α quenching phenomenology requires that the magnetic helicity in the small-scale fields approaches a nearly static, gauge independent state. To stress-test this steady state condition we choose a system with a uniform sign of kinetic helicity, so that the total magnetic helicity can reach a steady state value only through fluxes through the boundary, which are themselves suppressed by the velocity boundary conditions. Even with such a set up, the small-scale magnetic helicity is found to reach a steady state. In agreement with earlier work, the magnetic helicity fluxes of small-scale fields are found to be turbulently diffusive. By comparing results with and without halos, we show that artificial constraints on magnetic helicity at the boundary do not have a significant impact on the evolution of the magnetic helicity, except that “softer” (halo) boundary conditions give a lower energy of the saturated mean magnetic field.

Keywords: Solar dynamo – turbulence simulations – alpha effect – alpha quenching – magnetic helicity

1 Introduction

Stars with outer convection zones tend to possess magnetic fields that display spatio-temporal order with variations that are often cyclic and, in the case of the Sun, antisymmetric with respect to the equatorial plane. Simulations now begin to reproduce much of this behavior (see, e.g., Brown *et al.* 2010, Käpylä *et al.* 2010, Ghizaru *et al.* 2010). A useful tool for understanding the outcomes of such models is mean-field dynamo theory. A central ingredient of this theory is the α effect. This effect quantifies a component of the mean electromotive force that is proportional to the mean magnetic field (Moffatt 1978, Krause and Rädler 1980).

Mean-field theory gives meaningful predictions when to expect cyclic or steady solutions, and what the symmetry properties with respect to the equator are (Brandenburg 1998). Even in the nonlinear regime, the simple concept of α quenching, which reduces α locally via an algebraic function of the mean magnetic field, tends to give plausible results. However, under some circumstances, it becomes quite clear that this simple-minded approach must be wrong. Such a special case is that of a triply-periodic domain. Astrophysically speaking, such a model is quite unrealistic, but it is often employed in numerical simulations. It was also employed as the primary tool to compute α quenching from simulations (Cattaneo and Hughes 1996). These simulations suggest that α quenching would set in once the mean field becomes comparable to a small fraction ($R_m^{-1/2}$, where R_m is the magnetic Reynolds number) times the equipartition value. If this were true also for astrophysical bodies such as the Sun, the α effect could not be invoked for understanding the dynamics of the Sun’s magnetic field.

Later it became clear that there are counter examples to the simple idea that α is quenched just depending on the local field strength. Surprisingly, simulations later suggested that even in a triply-periodic domain a large-scale magnetic field can be generated that can even exceed the equipartition value (Brandenburg 2001). However, it would take a resistive time-scale to reach these field strengths, so there was still a problem. Around the same time, the idea emerged that open boundaries might help (Blackman and Field 2000a,b, Kleeorin *et al.* 2000, 2002). This is connected with the fact that an α effect dynamo produces magnetic helicity of opposite sign at large and small scales (Seehafer 1996, Ji 1999). The magnetic helicity

at small scales is an unwanted by-product that can feed back adversely on the dynamo. The resistively slow saturation phase in periodic-box simulations can then be understood in terms of the time it takes to dissipate this small-scale magnetic helicity. It is indeed a particular property of triply-periodic domains that magnetic helicity is strictly conserved at large magnetic Reynolds numbers. A possible remedy might then be to consider open domains that allow magnetic helicity fluxes.

The first simulations with open domains were not encouraging. While it was possible to reach saturation more quickly, the field was found to level off at a value that becomes progressively smaller at larger magnetic Reynolds numbers (Brandenburg and Dobler 2001, Brandenburg and Subramanian 2005a). A possible problem with these simulations might be the absence of magnetic helicity fluxes within the domain. Indeed, Brandenburg and Dobler (2001) considered a kinetic helicity distribution that was approximately uniform across the domain, so there were no gradients except in the immediate proximity of boundaries, where boundary conditions on the velocity prevent turbulent diffusion. The situation improved dramatically when simulations with shear were considered (Brandenburg 2005, Käpylä *et al.* 2008, Hughes and Proctor 2009). Shear provides not only an additional induction effect for the dynamo, but it might also lead to an additional source of magnetic helicity flux within the domain (Vishniac and Cho 2001, Subramanian and Brandenburg 2004, 2006). More recently it turned out that, even without shear, diffusion down the gradient of small-scale magnetic helicity could, at least in principle, help avoid vanishingly small saturation levels of the mean magnetic field when the magnetic Reynolds number becomes large (Brandenburg *et al.* 2009, Mitra *et al.* 2010).

An important goal of the present paper is to revisit this issue using direct simulations of turbulent dynamos without shear, and even with the same sign of magnetic helicity everywhere, but with a spatial modulation of the helicity within the domain. In other words, the level of turbulence is maintained at a high level throughout the domain, but the amount of swirl diminishes toward the boundaries. In most of the simulations we include a turbulent halo outside the dynamo domain where the Ohmic resistivity is enhanced. This might be important as several simple boundary conditions such as pseudo-vacuum (or vertical field) conditions fix the value of the magnetic helicity artificially, and if fluid motions through the boundary are prohibited, turbulent transport there is impossible.

Our simulations also allow us to make contact with nonlinear mean-field phenomenology where the evolution of the small-scale magnetic helicity is taken into account. This leads then to an evolution equation for an additional contribution to the α effect, α_M . This approach is referred to as dynamical α quenching. In the present paper we will also attempt to assess the validity of some of the corner stones of dynamical α quenching. Firstly, there is the magnetic α of Pouquet *et al.* (1976), where the fluctuating magnetic field generates an α_M that is proportional to the current helicity of the fluctuating field. This α_M counteracts the kinetic α , and so saturates the dynamo. Secondly there is magnetic helicity conservation which notes that the total magnetic helicity is nearly conserved under common conditions, and so the helicity in the fluctuating field can be related to the helicity in the large-scale field. Finally, there is the assumption that the mean current helicity of the fluctuating field is proportional to the mean magnetic helicity in the fluctuating field.

As noted above, a problematic prediction of dynamical α quenching is that rapid (exponential) growth of mean magnetic fields will be halted below equipartition with the turbulent energy. The export of small-scale helicity could provide a release from this constraint but will likely occur side-by-side with export of the mean field. The interplay between these effects can smother the dynamo even in the presence of small-scale helicity transport. Treatment of large-scale helicity transport proves significantly more complicated than that of the small-scale helicity, but we will draw some preliminary conclusions.

In Section 2 we discuss the dynamical α quenching phenomenology. In Section 3 we describe the numerical setup of the simulations whose results are analyzed in Section 4. Mean-field models of the systems are discussed in Section 5 and we conclude in Section 6.

2 Dynamical α quenching

We wish to use a mean-field approach to the saturation behavior of dynamos. In what follows our averages will be denoted by overbars and the fluctuating terms will be denoted by lower case symbols. In the

simulations we will be using planar xy averaging unless noted otherwise, so the mean magnetic vector potential is given by

$$\overline{\mathbf{A}}(z, t) = \int \int \mathbf{A}(x, y, z, t) dx dy / L_x L_y, \quad (1)$$

$$\mathbf{A} = \overline{\mathbf{A}} + \mathbf{a}, \quad (2)$$

so the mean magnetic field is $\overline{\mathbf{B}} = \nabla \times \overline{\mathbf{A}}$ and the mean current density is $\overline{\mathbf{J}} = \nabla \times \overline{\mathbf{B}} / \mu_0$, where μ_0 is the vacuum permeability. In the following we adopt units in which $\mu_0 = 1$. Throughout this paper we use the expressions ‘mean field’ and ‘large-scale field’ synonymously. Likewise, we refer to the ‘small-scale field’ as the ‘fluctuating field’.

We will work in the Weyl gauge (zero electrostatic potential, i.e. $\partial \mathbf{A} / \partial t = \mathbf{u} \times \mathbf{B} - \eta \mathbf{J}$), and assume that there is no mean velocity. We adopt the magnetic α prescription of Kleeorin and Ruzmaikin (1982). As such our mean-field theoretic equations are:

$$\frac{\partial \overline{\mathbf{B}}}{\partial t} = \nabla \times (\overline{\mathcal{E}} - \eta \overline{\mathbf{J}}), \quad (3)$$

$$\overline{\mathcal{E}} = \alpha \overline{\mathbf{B}} - \eta_t \overline{\mathbf{J}}, \quad (4)$$

$$\alpha = \alpha_K + \alpha_M, \quad (5)$$

$$\alpha_M = \frac{\tau}{3} \frac{\overline{\mathbf{j} \cdot \mathbf{b}}}{\mu_0 \rho} \simeq k_f^2 \frac{\tau}{3} \frac{\overline{\mathbf{a} \cdot \mathbf{b}}}{\mu_0 \rho} \simeq k_f^2 \frac{\eta_t}{B_{\text{eq}}^2} \overline{\mathbf{a} \cdot \mathbf{b}}, \quad (6)$$

where $\overline{\mathcal{E}} = \overline{\mathbf{u} \times \mathbf{b}}$ is the mean electromotive force, α_K is the kinetic α effect, $B_{\text{eq}}^2 \equiv \rho u_{\text{rms}}^2$ is a measure of the turbulent kinetic energy and $\eta_t \equiv \tau u_{\text{rms}}^2 / 3$ is the turbulent diffusivity. The parameter k_f is the wavenumber of the energy carrying scale of the turbulence. This α_M is taken to be the back-reaction component of α when it is split into kinetic and magnetic components (Pouquet *et al.* 1976).

Magnetic helicity conservation can be seen from the time evolution equation of the magnetic helicity density $h_T \equiv \mathbf{A} \cdot \mathbf{B}$,

$$\frac{\partial h_T}{\partial t} = -2\eta \mathbf{J} \cdot \mathbf{B} - \nabla \cdot \mathcal{F}_T, \quad (7)$$

where \mathcal{F}_T is the magnetic helicity flux. The subscript T refers to total field, which is composed of mean (m) and fluctuating (f) fields. In systems where the flux of magnetic helicity can be neglected (such as spatially homogeneous systems), and when the magnetic Reynolds number R_m is large enough (and therefore η small) the magnetic helicity will be nearly conserved. We define the large-scale and small-scale helicities as

$$\overline{h}_m \equiv \overline{\mathbf{A} \cdot \mathbf{B}}, \quad (8)$$

$$\overline{h}_f \equiv \overline{\mathbf{a} \cdot \mathbf{b}} = \overline{h}_T - \overline{h}_m. \quad (9)$$

Averaging Equation (7) we arrive at:

$$\frac{\partial \overline{h}_T}{\partial t} = \frac{\partial \overline{h}_m}{\partial t} + \frac{\partial \overline{h}_f}{\partial t} = -2\eta \overline{\mathbf{J} \cdot \mathbf{B}} - 2\eta \overline{\mathbf{j} \cdot \mathbf{b}} - \nabla \cdot \overline{\mathcal{F}}_T, \quad (10)$$

$$\frac{\partial \overline{h}_m}{\partial t} = 2\overline{\mathcal{E} \cdot \mathbf{B}} - 2\eta \overline{\mathbf{J} \cdot \mathbf{B}} - \nabla \cdot \overline{\mathcal{F}}_m, \quad (11)$$

$$\frac{\partial \overline{h}_f}{\partial t} = -2\overline{\mathcal{E} \cdot \mathbf{B}} - 2\eta \overline{\mathbf{j} \cdot \mathbf{b}} - \nabla \cdot \overline{\mathcal{F}}_f. \quad (12)$$

In the spirit of mean-field theory, we will scale the fluxes to gradients of mean quantities. We consider here only a diffusive helicity flux of the small-scale fields,

$$\overline{\mathcal{F}}_f \sim -\kappa_f \nabla \overline{h}_f, \quad (13)$$

while the flux of large-scale helicity will be discussed in greater detail in Section 4. In view of Equation (6), the evolution of \overline{h}_f is basically equivalent to the evolution of α_M .

3 Numerical setup

In this paper we present both direct numerical simulations and mean-field calculations. In both cases we use the PENCIL CODE¹, which is a modular high-order code (sixth order in space and third-order in time) for solving a large range of different partial differential equations.

We consider models with and without a halo. In both cases the horizontal extent of the domain is $L_x \times L_y$ with equal side lengths $L_x = L_y \equiv L$, with periodic boundaries. In cases without a halo the vertical extent of the domain is $L_z = L$ while in cases with a halo we choose $L_z = 2L$. In the following we measure length in units of k_1^{-1} , where $k_1 = 2\pi/L$ is the minimal horizontal wavenumber. We will define our magnetic Reynolds number as

$$R_m \equiv u_{\text{rms}}/\eta k_f, \quad (14)$$

where we assume that the wavenumber of the forcing is also the wavenumber of the turbulence, and use a scale separation ratio $k_f/k_1 = 3$.

At the top and bottom, we impose stress-free velocity conditions with $u_z = 0 = \partial u_x/\partial z = \partial u_y/\partial z$. At the top and bottom we impose a ‘‘vertical field’’ condition, $A_z = \partial A_x/\partial z = \partial A_y/\partial z$. This condition imposes $B_x = B_y = 0$ and hence $\mathbf{A} \cdot \mathbf{B} = 0$. As this condition on magnetic helicity may be artificial, and the velocity boundary condition constrains turbulent transport into the boundary, we include buffer ‘‘halos’’, such that the microscopic magnetic diffusivity is given by

$$\eta = \begin{cases} \eta_0 & -\pi \leq k_1 z \leq \pi \\ \eta_H & |k_1 z| > \pi, \end{cases} \quad (15)$$

where $\eta_H \gg \eta_0$. We include forced turbulence, with uniform amplitude and wavenumber k_f , but a relative helicity $\sigma = (\nabla \times \mathbf{f} \cdot \mathbf{f})/k_f f^2$ of

$$\sigma = \begin{cases} \cos k_1 z/2 & -\pi \leq z \leq \pi \\ 0 & |k_1 z| > \pi. \end{cases} \quad (16)$$

For detailed about the implementation of a forcing function with variable helicity we refer to the paper by Haugen *et al.* (2004).

The above system is interesting from a dynamical α perspective as it contains several contrasting elements. Unlike Mitra *et al.* (2010), the forcing helicity is all of one sign, and so we expect the magnetic and current helicities to also be of one sign. This implies that the production term in Equation (7) be finite even after volume averaging, and there may never be a final steady state for the magnetic helicity. Further, fluxes through the actual boundaries are reduced through the velocity boundary conditions as well as the resistive destruction of the field in the halos. It is not clear whether the magnetic vector potential will even have a final steady solution. An example of an unsteady magnetic helicity in an otherwise fully steady dynamo was presented in Fig. 2 of Brandenburg *et al.* (2002).

¹<http://pencil-code.googlecode.com>

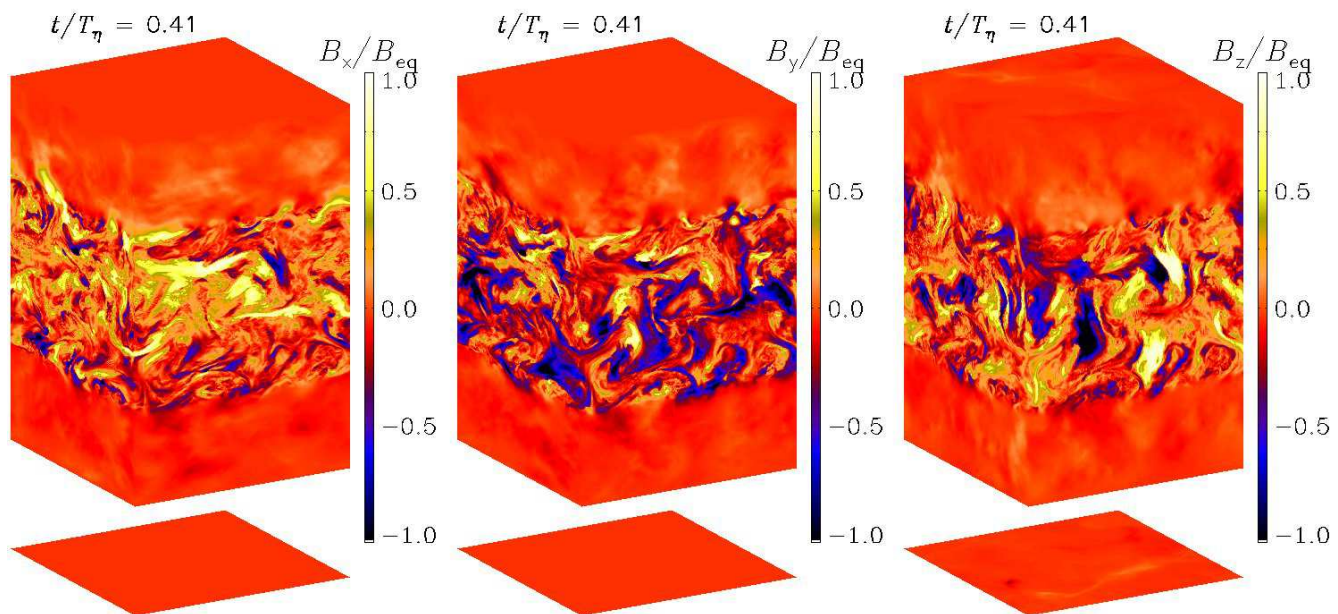


Figure 1. Visualizations of each of the three components of \mathbf{B} on the periphery of the computational domain, for a run with $R_m = 1300$ using $256 \times 256 \times 512$ mesh points. The lower planes show the field at the lower boundary, where it is quite weak. Note the presence of mild overshoot into the upper and lower halos, where $\eta_H = 250\eta_0$. In the bulk of the domain the x and y components show a large-scale field with variation in the z direction, while B_z does not show a systematic mean field.

The main difference compared with earlier work is that in Mitra *et al.* (2010) there was an equator at $z = 0$ with kinetic helicity of opposite sign for $z < 0$. Consequently, also \bar{h}_f changes sign, allowing an efficient exchange of magnetic helicity by the turbulence. The present model is more similar to that of Brandenburg and Dobler (2001), except that there the kinetic helicity profile was flat in the bulk of the dynamo interior and it dropped to zero only immediately at the boundary of the domain, or gradually so in those cases where a conducting non-turbulent halo was included.

The helicity in the halos, as noted above, will be suppressed by the low conductivity, as we expect small-scale helicity transport away from the active central region. A strong, rapidly achieved final mean-field would indicate that flux of small scale helicity provides a clear escape from dynamical α quenching. Finally, a clear difference between halo simulations and simulations without a halo will be evidence that the boundary conditions are generating artificial constraints. If these differences are visible in the field itself (as opposed to the vector potential), they are likely due to the reduced turbulent diffusion into the boundary.

Mean quantities are calculated from time series over a long stretch of time where the relevant quantities are approximately stationary in the statistical sense. We use the time series further to calculate lower bounds on the error bars as the maximum departure between these averages and the averages obtained from any of the three equally long subsections of the full time series.

4 Results of simulations

In the statistically steady state, the magnetic field shows a large-scale magnetic field that varies in the z direction; see Figure 1. It is therefore meaningful to describe the dynamics of this large-scale field by using horizontal averages as noted in Section 2. We will use angular brackets and capitals to refer to volume averages over the volume $V = L_x L_y L'_z$, where $L'_z = z_2 - z_1$ and $-z_1 = z_2 = 2k_1^{-1}$. This will mark the

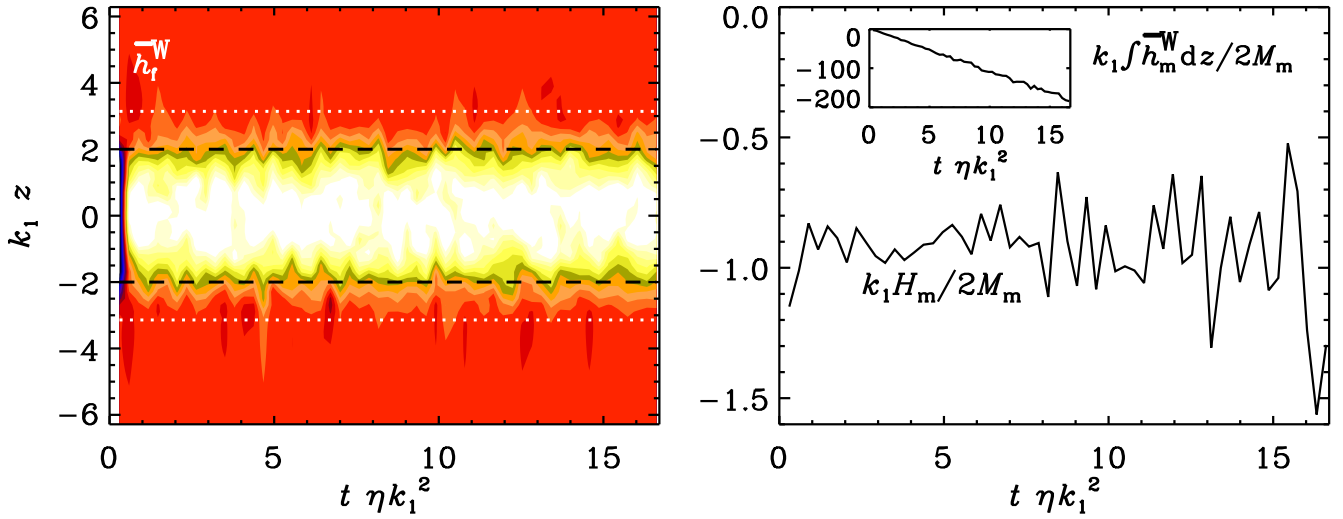


Figure 2. Magnetic helicity density of the small-scale magnetic field in the Weyl gauge, $\overline{h_f^W}$, as a function of z and t (left-hand panel), and the gauge-independent magnetic helicity of the large-scale field, H_m in units of $2M_m/k_1$ (right-hand panel), for Run H3 with $\eta_H = 100\eta_0$. For comparison, the Weyl-gauged magnetic helicity of the large-scale field is shown in the inset. The data are averaged over regular time intervals of about 0.3 diffusive times, which also explains the absence of data at $t = 0$.

boundaries of a smaller domain well within the dynamo region. Thus, we write

$$H(t) = \langle h \rangle_V V = \frac{1}{L_x L_y L'_z} \int \int \int h(x, y, z, t) dx dy dz = \frac{1}{L'_z} \int \overline{h}_\Gamma(z, t) dz, \quad (17)$$

where h and H could stand for H_m and h_m , or for H_f and h_f , for example. We note, however, that these quantities may be gauge-dependent. We also define the magnetic energy of the mean field as $M_m = \langle \overline{\mathbf{B}}^2 / 2 \rangle V$.

4.1 Small-scale helicity flux

We define the magnetic helicity densities for the mean and fluctuating fields as

$$\overline{h}_m^W = \overline{\mathbf{A}} \cdot \overline{\mathbf{B}}, \quad \overline{h}_f^W = \overline{\mathbf{a}} \cdot \overline{\mathbf{b}}. \quad (18)$$

The superscript W indicates that we are working in the Weyl gauge modulo possible influences of the boundary conditions that have been mitigated through the use of halos. It turns out that \overline{h}_m^W has a systematic variation in time while \overline{h}_f^W does not; see Figure 2. It makes therefore sense to average the evolution equation for \overline{h}_f^W in time, so we have (Mitra *et al.* 2010)

$$\left\langle \frac{\partial \overline{h}_f^W}{\partial t} \right\rangle_T = 0 = -2 \langle \overline{\boldsymbol{\mathcal{E}}} \cdot \overline{\mathbf{B}} \rangle_T - 2\eta \langle \mathbf{j} \cdot \mathbf{b} \rangle_T - \langle \nabla \cdot \overline{\mathcal{F}}_f^W \rangle_T, \quad (19)$$

where subscripts indicate time averaging over the interval T . In the Weyl gauge the magnetic helicity flux of the small-scale field is given by $\overline{\mathcal{F}}_f^W = \overline{\mathbf{e}} \times \overline{\mathbf{a}}$, where $\mathbf{e} = \mathbf{E} - \overline{\mathbf{E}}$ is the electric field for the fluctuating quantities. Given that the first two terms on the rhs of Equation (19) are gauge-invariant, $\langle \nabla \cdot \overline{\mathcal{F}}_f \rangle_T$ must also be gauge-invariant, so we can drop the superscript W and note that, in the particular case at hand, we have $\langle \nabla \cdot \overline{\mathcal{F}}_f^W \rangle_T = \langle \nabla \cdot \overline{\mathcal{F}}_f \rangle_T$. We emphasize that $\langle \nabla \cdot \overline{\mathcal{F}}_f \rangle_T$ is still a function of z .

4.2 Large-scale helicity flux

In order to assess the full magnetic helicity budget, we also need to take the magnetic helicity of the mean field into account. Since \overline{h}_m^W is time-dependent, it is not possible to invoke a similar argument as for \overline{h}_f^W . We are therefore forced to abandon a detailed analysis of the z dependence of the magnetic helicity budget and restrict ourselves to the analysis of the volume-integrated magnetic helicity, H_m , and its corresponding flux divergence, Q_m , using the gauge-invariant prescription of Brandenburg and Dobler (2001) for the volume in $z_1 \leq z \leq z_2$,

$$H_m(t) = \int_{z_1}^{z_2} \overline{h}_m^W(z, t) dz + \overline{\mathbf{A}}(z_1, t) \times \overline{\mathbf{A}}(z_2, t), \quad (20)$$

and

$$Q_m(t) = -[\overline{\mathbf{E}}(z_1, t) + \overline{\mathbf{E}}(z_2, t)] \cdot \int_{z_1}^{z_2} \overline{\mathbf{B}}(z, t) dz, \quad (21)$$

where $\overline{\mathbf{E}} = \eta \overline{\mathbf{J}} - \overline{\mathcal{E}}$ is the mean electric field expressed in terms of horizontally averaged Ohm's law. Note that H_m and Q_m obey the evolution equation

$$\frac{dH_m}{dt} = 2 \int_{z_1}^{z_2} \overline{\mathcal{E}} \cdot \overline{\mathbf{B}} dz - 2\eta \int_{z_1}^{z_2} \overline{\mathbf{J}} \cdot \overline{\mathbf{B}} dz - Q_m. \quad (22)$$

It turns out that, unlike \overline{h}_m^W and its volume-integral, H_m is statistically steady (see Figure 2), so we may now also average Equation (22) over time.

4.3 Magnetic helicity budgets

In Table 1, we summarize the helicity budgets, namely the six terms on the rhs of Equations (19) and (22), of which the $2\langle \overline{\mathcal{E}} \cdot \overline{\mathbf{B}} \rangle$ term occurs twice. We have used here the more descriptive symbol $\langle \nabla \cdot \overline{\mathcal{F}}_m \rangle_{VT} \equiv Q_m / (z_2 - z_1)$ for the flux divergence of the helicity of the mean field. In order to simplify the notation, we drop from now on the subscripts VT and define angular brackets without subscripts as combined averages over a long enough time span and over the volume V in $z_1 \leq z \leq z_2$, where again, $-z_1 = z_2 = 2k_1^{-1}$.

Table 1. Summary of the volume and time averaged terms on the rhs of Equations (19) and (22), normalized by $\eta_{t0} B_{\text{eq}}^2$, while $\langle \overline{\mathbf{B}}^2 \rangle$ is normalized by B_{eq}^2 . Runs H1–6 refer to systems with a poorly conducting halo with $\eta_H / \eta_0 \approx R_m$, while in Runs VF1–6 refer to systems without a halo and a vertical field boundary condition at $|k_1 z| = \pi$. The data for Run H6 are given for completeness, but it has not run long enough to have satisfactory statistics.

Run	R_m	$\langle \overline{\mathbf{B}}^2 \rangle$	$2\langle \overline{\mathcal{E}} \cdot \overline{\mathbf{B}} \rangle$	$2\eta \langle \overline{\mathbf{J}} \cdot \overline{\mathbf{B}} \rangle$	$2\eta \langle \overline{\mathbf{j}} \cdot \overline{\mathbf{b}} \rangle$	$\langle \nabla \cdot \overline{\mathcal{F}}_m \rangle$	$\langle \nabla \cdot \overline{\mathcal{F}}_f \rangle$
H1	20	0.56	-0.423 ± 0.003	-0.068 ± 0.000	0.408 ± 0.002	-0.360 ± 0.006	0.018 ± 0.013
H2	50	0.33	-0.208 ± 0.003	-0.018 ± 0.000	0.190 ± 0.001	-0.192 ± 0.005	0.012 ± 0.004
H3	140	0.15	-0.086 ± 0.003	-0.003 ± 0.000	0.078 ± 0.001	-0.079 ± 0.005	0.005 ± 0.001
H4	270	0.12	-0.047 ± 0.002	-0.001 ± 0.000	0.041 ± 0.000	-0.046 ± 0.001	0.003 ± 0.000
H5	520	0.08	-0.024 ± 0.000	-0.000 ± 0.000	0.020 ± 0.000	-0.024 ± 0.001	0.002 ± 0.000
H6	1280	0.08	-0.029 ± 0.023	-0.000 ± 0.000	0.009 ± 0.000	-0.007 ± 0.007	-0.007 ± 0.004
VF1	10	0.62	-0.823 ± 0.011	-0.163 ± 0.002	0.822 ± 0.005	-0.669 ± 0.005	-0.000 ± 0.012
VF2	20	0.43	-0.434 ± 0.004	-0.051 ± 0.002	0.436 ± 0.003	-0.400 ± 0.005	0.002 ± 0.026
VF3	50	0.32	-0.250 ± 0.013	-0.019 ± 0.001	0.247 ± 0.002	-0.224 ± 0.009	0.006 ± 0.012
VF4	120	0.28	-0.138 ± 0.009	-0.007 ± 0.000	0.134 ± 0.001	-0.143 ± 0.004	0.001 ± 0.008
VF5	220	0.25	-0.091 ± 0.002	-0.003 ± 0.000	0.082 ± 0.001	-0.086 ± 0.002	0.004 ± 0.003
VF6	400	0.15	-0.053 ± 0.002	-0.001 ± 0.000	0.046 ± 0.000	-0.052 ± 0.001	0.005 ± 0.002

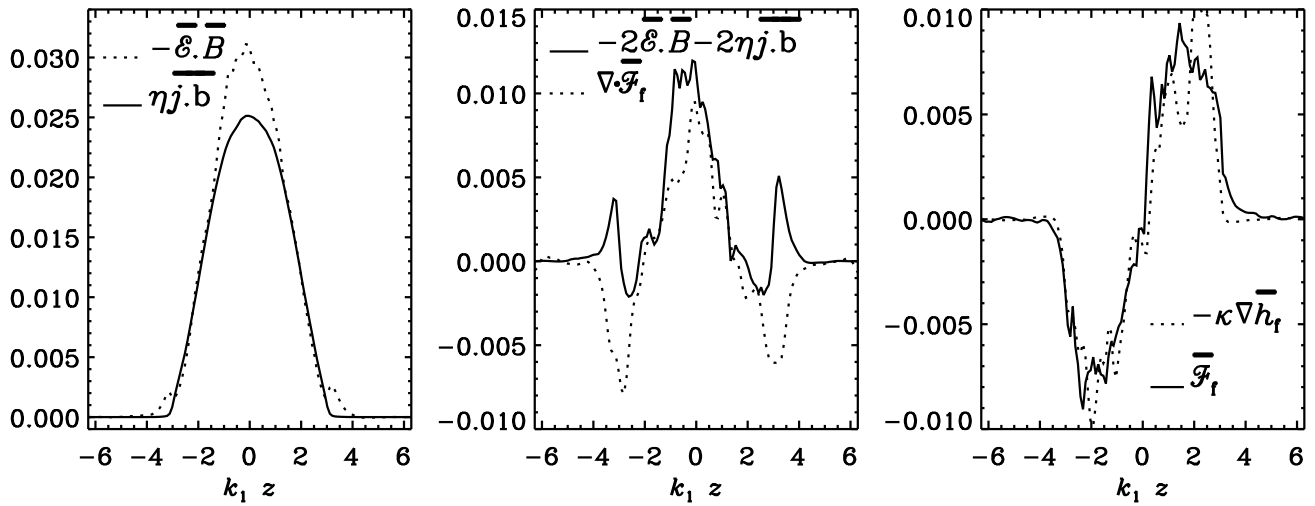


Figure 3. Time-averaged terms on the right-hand side of Equation (19) for Run H4, $\langle \overline{\mathcal{E}} \cdot \overline{\mathbf{B}} \rangle_T$ and $\eta \langle \overline{\mathbf{j}} \cdot \overline{\mathbf{b}} \rangle_T$ (left panel), the difference between these terms compared with the magnetic helicity flux divergence of small-scale fields $\langle \nabla \cdot \overline{\mathcal{F}}_f^W \rangle_T$ (middle panel), and the flux itself compared with the Fickian diffusion ansatz (right-hand panel). The fluxes are given in units of $\eta_0 B_{\text{eq}}^2$ and the flux divergence is given in units of $k_1 \eta_0 B_{\text{eq}}^2$.

The results given in Table 1 show that $2\langle \overline{\mathcal{E}} \cdot \overline{\mathbf{B}} \rangle$ is balanced essentially by $\langle \nabla \cdot \overline{\mathcal{F}}_m \rangle$, because $\eta \langle \overline{\mathbf{j}} \cdot \overline{\mathbf{b}} \rangle$ is small. On the other hand, for the magnetic Reynolds numbers considered here ($R_m \lesssim 500$), the $2\eta \langle \overline{\mathbf{j}} \cdot \overline{\mathbf{b}} \rangle$ term is still quite large, and contributes mainly to balancing $-2\langle \overline{\mathcal{E}} \cdot \overline{\mathbf{B}} \rangle$ in the magnetic helicity balance for the fluctuating field. The other (smaller) contribution comes from $\langle \nabla \cdot \overline{\mathcal{F}}_f \rangle$. This result is quite similar to that of Mitra *et al.* (2010) for the case of a linearly varying kinetic helicity profile, where it was found that, even though most of $\langle \overline{\mathcal{E}} \cdot \overline{\mathbf{B}} \rangle$ is still balanced by $\eta \langle \overline{\mathbf{j}} \cdot \overline{\mathbf{b}} \rangle$, both $\langle \overline{\mathcal{E}} \cdot \overline{\mathbf{B}} \rangle$ and $\langle \nabla \cdot \overline{\mathcal{F}}_f \rangle$ vary little with R_m and must eventually dominate over $\eta \langle \overline{\mathbf{j}} \cdot \overline{\mathbf{b}} \rangle$ as η decreases with increasing R_m . This was estimated to happen at $R_m = 10^3 \dots 10^4$. In the model presented here, this is not so obvious, because $\langle \overline{\mathcal{E}} \cdot \overline{\mathbf{B}} \rangle$ shows still a rapid decline with increasing R_m . This may be a consequence of the fact that also $\overline{\mathbf{B}}^2$ declines still quite rapidly with increasing R_m , which indicates that the quenching is R_m -dependent, at least for the values of R_m considered here.

Note that the final field strength for systems without halos tends to be higher than for systems with halos: turbulent transport of the mean field out of the active region plays an important role. This implies that the turbulent flux of magnetic helicity from small-scale fields has a weaker effect on the final strength of the mean field than the turbulent flux of the mean field itself.

Note also that the total helicities H_m and H_f show little difference in the two setups, suggesting that the artificially imposed $h = 0$ constraint on the boundary is not generating spurious results.

4.4 Magnetic helicity fluxes

In Table 2 we collect results for the magnetic helicity flux divergence. The profile of the flux of magnetic helicity from the small-scale magnetic field, $\overline{\mathcal{F}}_f$, is reasonably well described by a Fickian diffusion ansatz. In Figure 3 we show the profiles of $\langle \overline{\mathcal{E}} \cdot \overline{\mathbf{B}} \rangle$ and $\eta \langle \overline{\mathbf{j}} \cdot \overline{\mathbf{b}} \rangle$, compare the residual $2\langle \overline{\mathcal{E}} \cdot \overline{\mathbf{B}} \rangle - 2\eta \langle \overline{\mathbf{j}} \cdot \overline{\mathbf{b}} \rangle$ with the divergence of the magnetic helicity flux, and finally compare the flux $\overline{\mathcal{F}}_f = \overline{\mathbf{e}} \times \overline{\mathbf{a}}$ with that obtained from the diffusion approximation, $-\kappa_f \nabla \overline{h}_f$.

There are several additional points to be noted about the simulation results. Firstly, based on earlier results for triply-periodic domains one expects that H_m and H_f have the opposite sign, which is indeed always the case. Furthermore, we expect that the current helicity of the mean fields, $C_m \equiv \langle \overline{\mathbf{j}} \cdot \overline{\mathbf{B}} \rangle$, and H_m have the same sign and that $C_m/H_m \approx k_1^2$. This is indeed the case, except that the simulations give about half or less than the naively expected value for C_m/H_m . This indicates that the large-scale magnetic field is not fully helical, a potential reason for the modest mean-field saturation strength even in the presence of a magnetic helicity flux of small-scale fields. Likewise, one expects that C_f and H_f have again the same

sign. Again, this is borne out by the simulations, but the ratio $C_f/k_f^2 H_f$ is typically 3–5 times larger than the expected value of unity. This may well be a consequence of the presence of a finite flux divergence of magnetic helicity of small-scale fields.

Finally, we find that the sign of the flux divergence of magnetic helicity density of fluctuating and mean magnetic fields has the same sign as the respective magnetic helicities themselves. This is generally the case and is well motivated by the Fickian diffusion ansatz. Given that that we find $\kappa_f \approx 0.3\eta_{t0}$, we should expect that $Q_f/\eta_{t0}k_1^2 H_f$ is also about 0.3, but the real value is only 0.1. On the other hand $Q_m/\eta_{t0}k_1^2 H_m$ varies between 0.2 and 0.7, but tends to decrease with increasing values of R_m , although it remains above $Q_f/\eta_{t0}k_1^2 H_f$ and may be approaching it from above. As long as the transport of large-scale helicity has a larger transport coefficient than that of the small-scale helicity, we expect that the small-scale helicity transport will not result in larger helical mean field strengths even though it allows for a stronger post-kinematic α effect (Brandenburg and Subramanian 2005a).

The complication that $\eta\langle\mathbf{J}\cdot\mathbf{B}\rangle$ is not small even for the largest R_m should not be forgotten. The total helicity being forced, and eventually even the halo ‘buffer’ zones will transmit information to the boundary. It is therefore not clear how well a Fickian diffusion ansatz is justified for the helicity of the mean magnetic field.

5 Connection with mean-field models

In order to perform mean-field simulations, we need to include all the relevant turbulent transport coefficients. A robust tool for extracting these coefficients from simulation is the test-field method of Schrunner *et al.* (2005, 2007); for applications to time-dependence turbulence see Brandenburg *et al.* (2008a,b). We apply this technique both to the kinematic and to the nonlinear stage using the so-called quasi-kinematic test-field method Brandenburg *et al.* (2008c); for a justification of it see Rheinhardt and Brandenburg (2010). In Figure 4 we show not only the values of α and η_t as determined by the test-field method, but also the γ and δ effects in the more general expression

$$\overline{\mathcal{E}} = \alpha\overline{\mathbf{B}} + \gamma\hat{\mathbf{z}} \times \overline{\mathbf{B}} - \eta_t\overline{\mathbf{J}} + \delta\hat{\mathbf{z}} \times \overline{\mathbf{J}}. \quad (23)$$

As expected, the latter are negligible. Interestingly, we see evidence of quenching of η_t in the active region, even though the mean-field is well below equipartition ($\langle\overline{\mathbf{B}}^2\rangle = 0.1B_{\text{eq}}^2$). Further, we see an approximately 2-fold reduction both in α and in η_t .

In Figure 5 we compare the evolution of $\langle\overline{\mathbf{B}}^2\rangle/B_{\text{eq}}^2$ for the direct simulation with the solution of the corresponding mean-field model. There is excellent agreement in the final saturation level, and in both

Table 2. Normalized values of magnetic helicity, current helicity, and magnetic helicity flux divergence both for small-scale and large-scale magnetic fields.

Run	R_m	$k_1 H_m / 2M_m$	$C_m / k_1^2 H_m$	$Q_m / \eta_{t0} k_1^2 H_m$	$k_1 H_f / 2M_m$	$C_f / k_f^2 H_f$	$Q_f / \eta_{t0} k_1^2 H_f$
H1	20	-0.94 ± 0.02	0.54 ± 0.02	0.69 ± 0.01	0.15 ± 0.00	2.05 ± 0.04	0.21 ± 0.15
H2	50	-0.89 ± 0.01	0.56 ± 0.01	0.68 ± 0.02	0.21 ± 0.01	2.50 ± 0.12	0.18 ± 0.07
H3	140	-0.93 ± 0.06	0.51 ± 0.01	0.55 ± 0.03	0.34 ± 0.00	3.02 ± 0.06	0.08 ± 0.02
H4	270	-0.97 ± 0.02	0.50 ± 0.01	0.41 ± 0.01	0.38 ± 0.00	4.29 ± 0.07	0.08 ± 0.01
H5	520	-0.90 ± 0.02	0.53 ± 0.01	0.34 ± 0.01	0.46 ± 0.00	4.96 ± 0.09	0.07 ± 0.01
H6	1280	-1.30 ± 0.01	0.36 ± 0.02	0.08 ± 0.07	0.36 ± 0.04	6.68 ± 1.40	-0.15 ± 0.18
VF1	10	-2.47 ± 0.45	0.20 ± 0.03	0.45 ± 0.08	0.11 ± 0.02	2.67 ± 0.52	-0.21 ± 0.36
VF2	20	-2.40 ± 0.43	0.21 ± 0.03	0.40 ± 0.08	0.16 ± 0.02	2.69 ± 0.31	0.02 ± 0.40
VF3	50	-2.26 ± 0.37	0.22 ± 0.03	0.31 ± 0.07	0.24 ± 0.03	2.68 ± 0.26	0.06 ± 0.14
VF4	120	-1.82 ± 0.28	0.27 ± 0.04	0.29 ± 0.04	0.28 ± 0.01	3.49 ± 0.07	0.02 ± 0.10
VF5	220	-1.84 ± 0.32	0.26 ± 0.05	0.19 ± 0.04	0.32 ± 0.00	3.83 ± 0.07	0.06 ± 0.04
VF6	400	-1.49 ± 0.23	0.32 ± 0.04	0.23 ± 0.04	0.43 ± 0.01	4.76 ± 0.06	0.07 ± 0.04

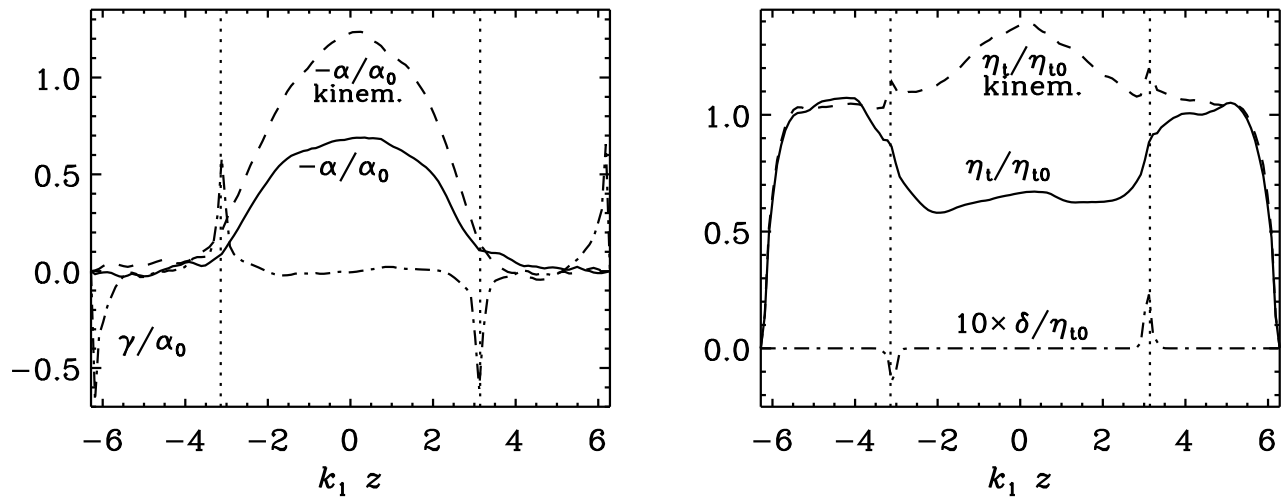


Figure 4. Profiles of α and η_t for Run H4 for the saturated case (solid lines) and the kinematic case (dashed lines), obtained using the test-field method. In the left and right panels, we also show γ and δ , respectively.

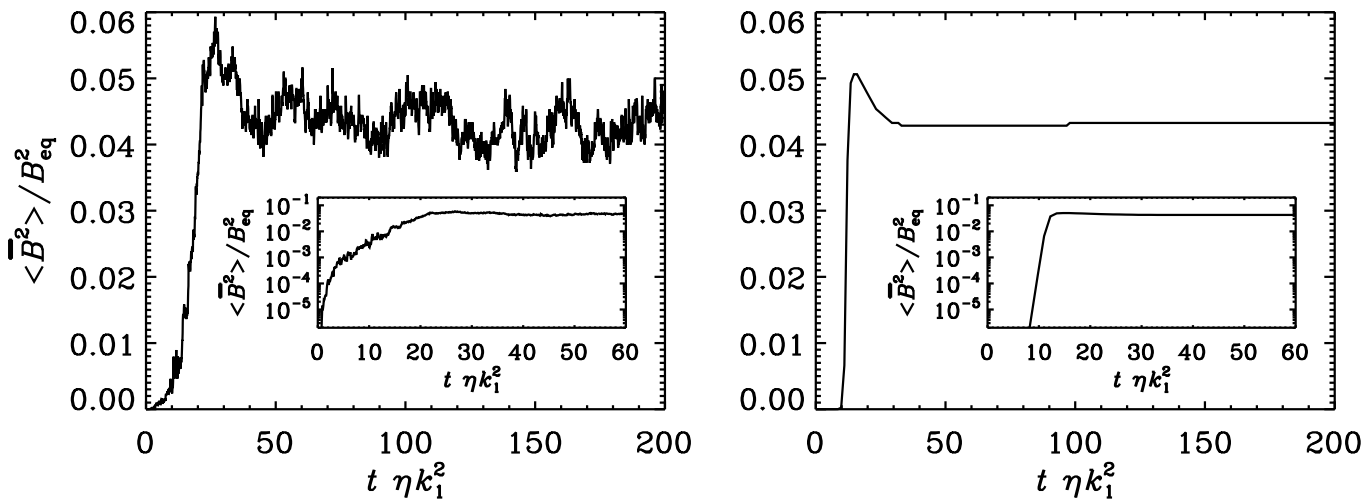


Figure 5. Comparison between the saturation behavior in the simulation (left) and the mean-field model (right) for the same parameters: $R_m/3 = 100$, $C_\alpha = 3$. Magnetic helicity flux and its fit in terms of a Fickian diffusion law, for Run H4.

cases the amplitude overshoots slightly before settling at a somewhat lower value, but the kinematic growth rate is much faster in the mean-field model than in the simulation. This discrepancy is not yet well understood and should be reconsidered in future work. Perhaps significantly, the rise time of the mean field is rapid even in terms of the turbulent turnover time. This means that memory effects become important (Hubbard and Brandenburg 2009), and that the actual growth rate would be reduced compared with that obtained from simple estimates. The overshoot may simply be an artifact of the finite time it takes the system to convert mean fields into correlated small-scale fields, which is not included in the mean-field model.

6 Conclusions

Confirming earlier work of Mitra *et al.* (2010), we have demonstrated the existence of a diffusive flux $\overline{\mathcal{F}}_f$ of mean magnetic helicity of the small-scale field. In the present case, however, the Weyl-gauged magnetic helicity of the large-scale field never reaches a steady state. Nevertheless, the magnetic helicity density of the small-scale magnetic field is found to be statistically steady, so the corresponding magnetic helicity flux

must be gauge-independent (Mitra *et al.* 2010). This supports the validity of using the small-scale magnetic helicity as a meaningful proxy for the small-scale current helicity, and hence the magnetic correction to the α effect.

Understanding the transport of magnetic helicity of the large-scale field, $\overline{\mathcal{F}}_m$, would be useful for creating analytic post-kinematic models. Although we have not converged on a formula for this flux, it is certainly finite and apparently R_m dependent. It is not yet clear whether this flux will converge to a diffusive one for large R_m . Our mean-field simulations reproduce the final field strength well, reinforcing the conclusion that post-kinematic dynamical α quenching can be used as part of a mean-field simulation.

The preliminary evidence on the use of small-scale helicity fluxes to escape the small predicted post-kinematic mean fields is negative: the observed flux of large-scale helicity, while poorly modeled, is larger than the flux of the small-scale helicity. If this holds for larger R_m , it would have the unfortunate result of closing escape holes from α quenching opened by $\overline{\mathcal{F}}_f$, but would also imply that dynamo systems with more realistic profiles than simple homogeneity will reach R_m independent behavior for high but currently nearly numerically achievable R_m . It is likely that conclusive evidence for or against R_m -dependent quenching requires values of R_m in the range between 10^3 and 10^4 (Brandenburg *et al.* 2009, Mitra *et al.* 2010).

Acknowledgements

We thank Petri Käpylä for detailed suggestions that have helped to improve our paper. We acknowledge the allocation of computing resources provided by the Swedish National Allocations Committee at the Center for Parallel Computers at the Royal Institute of Technology in Stockholm and the National Supercomputer Centers in Linköping as well as the Norwegian National Allocations Committee at the Bergen Center for Computational Science. This work was supported in part by the European Research Council under the AstroDyn Research Project No. 227952 and the Swedish Research Council Grant No. 621-2007-4064.

REFERENCES

- Blackman, E.G. and Field, G. B., “Constraints on the magnitude of α in dynamo theory,” *Astrophys. J.* **534**, 984-988 (2000a).
- Blackman, E.G. and Field, G. B., “Coronal activity from dynamos in astrophysical rotators,” *Monthly Notices Roy. Astron. Soc.* **318**, 724-724 (2000b).
- Brandenburg, A., “Disc Turbulence and Viscosity,” In *Theory of Black Hole Accretion Discs* (ed. M. A. Abramowicz, G. Björnsson and J. E. Pringle), pp. 61-86. Cambridge University Press (1998).
- Brandenburg, A., “The inverse cascade and nonlinear alpha-effect in simulations of isotropic helical hydromagnetic turbulence,” *Astrophys. J.* **550**, 824-840 (2001).
- Brandenburg, A., “The case for a distributed solar dynamo shaped by near-surface shear,” *Astrophys. J.* **625**, 539-547 (2005).
- Brandenburg, A. and Dobler, W., “Large scale dynamos with helicity loss through boundaries,” *Astron. Astrophys.* **369**, 329-338 (2001).
- Brandenburg, A. and Subramanian, K., “Strong mean field dynamos require supercritical helicity fluxes,” *Astron. Nachr.* **326**, 400-408 (2005a).
- Brandenburg, A. and Subramanian, K., “Astrophysical magnetic fields and nonlinear dynamo theory,” *Phys. Rep.* **417**, 1-209 (2005b).
- Brandenburg, A., Dobler, W. and Subramanian, K., “Magnetic helicity in stellar dynamos: new numerical experiments,” *Astron. Nachr.* **323**, 99-122 (2002).
- Brandenburg, A., Rädler, K.-H. and Schinner, M., “Scale dependence of alpha effect and turbulent diffusivity,” *Astron. Astrophys.* **482**, 739-746 (2008a).
- Brandenburg, A., Rädler, K.-H., Rheinhardt, M. and Käpylä, P. J., “Magnetic diffusivity tensor and dynamo effects in rotating and shearing turbulence,” *Astrophys. J.* **676**, 740-751 (2008b).
- Brandenburg, A., Rädler, K.-H., Rheinhardt, M. and Subramanian, K., “Magnetic quenching of alpha and diffusivity tensors in helical turbulence,” *Astrophys. J. Letters* **687**, L49-L52 (2008).

- Brandenburg, A., Candelaresi, S. and Chatterjee, P., "Small-scale magnetic helicity losses from a mean-field dynamo," *Monthly Notices Roy. Astron. Soc.* **398**, 1414-1422 (2009).
- Brown, B. P., Browning, M. K., Brun, A. S., Miesch, M. S., Toomre, J., "Persistent Magnetic Wreaths in a Rapidly Rotating Sun," *Astrophys. J.* **711**, 424-438 (2010).
- Cattaneo, F. and Hughes, D.W., "Nonlinear saturation of the turbulent alpha effect," *Phys. Rev. E* **54**, R4532-R4535 (1996).
- Ghizaru, M., Charbonneau, P. and Smolarkiewicz, P.K., 2010 (preprint)
- Haugen, N. E. L., Brandenburg, A. and Dobler, W., "Simulations of nonhelical hydromagnetic turbulence," *Phys. Rev.* **70**, 016308 (2004).
- Hubbard, A. and Brandenburg, A., "Memory effects in turbulent transport," *Astrophys. J.* **706**, 712-726 (2009).
- Hughes, D. W. and Proctor, M. R. E., "Large-scale dynamo action driven by velocity shear and rotating convection," *Phys. Rev. Letters* **102**, 044501 (2009).
- Ji, H., "Turbulent dynamos and magnetic helicity," *Phys. Rev. Letters* **83**, 3198-3201 (1999).
- Moffatt, H. K. *Magnetic field generation in electrically conducting fluids*. Cambridge University Press, Cambridge (1978).
- Kleorin, N., Moss, D., Rogachevskii, I. and Sokoloff, D., "Helicity balance and steady-state strength of the dynamo generated galactic magnetic field," *Astron. Astrophys.* **361**, L5-L8 (2000).
- Kleorin, N., Moss, D., Rogachevskii, I. and Sokoloff, D., "The role of magnetic helicity transport in nonlinear galactic dynamos," *Astron. Astrophys.* **387**, 453-462 (2002).
- Kleorin, N. I. and Ruzmaikin, A. A., "Dynamics of the average turbulent helicity in a magnetic field," *Magnetohydrodynamics* **18**, 116-122 (1982). Translation from *Magnitnaya Gidrodinamika*, 2, pp. 17-24 (1982)
- Krause, F. and Rädler, K.-H. *Mean-field magnetohydrodynamics and dynamo theory*. Pergamon Press, Oxford (1980).
- Käpylä, P. J., Korpi, M. J. and Brandenburg, A., "Large-scale dynamos in turbulent convection with shear," *Astron. Astrophys.* **491**, 353-362 (2008).
- Käpylä, P. J., Korpi, M. J. and Brandenburg, A., Mitra, D., and Tavakol, R., "Convective dynamos in spherical wedge geometry," *Astron. Nachr.* **331**, 73-81 (2010).
- Mitra, D., Candelaresi, S., Chatterjee, P., Tavakol, R. and Brandenburg, A., "Equatorial magnetic helicity flux in simulations with different gauges," *Astron. Nachr.* **331**, 130-135 (2010).
- Pouquet, A., Frisch, U., and Léorat, J., "Strong MHD helical turbulence and the nonlinear dynamo effect," *J. Fluid Mech.* **77**, 321-354 (1976).
- Rheinhardt, M. and Brandenburg, A. 2010 "Test-field method for mean-field coefficients with MHD background," *Astron. Astrophys.* (submitted). Available as e-print arXiv:1004.0689.
- Schrinner, M., Rädler, K.-H., Schmitt, D., Rheinhardt, M., Christensen, U., "Mean-field view on rotating magnetoconvection and a geodynamo model," *Astron. Nachr.* **326**, 245-249 (2005).
- Schrinner, M., Rädler, K.-H., Schmitt, D., Rheinhardt, M., Christensen, U. R., "Mean-field concept and direct numerical simulations of rotating magnetoconvection and the geodynamo," *Geophys. Astrophys. Fluid Dynam.* **101**, 81-116 (2007).
- Seehafer, N., "Nature of the α effect in magnetohydrodynamics," *Phys. Rev. E* **53**, 1283-1286 (1996).
- Subramanian, K. and Brandenburg, A., "Nonlinear current helicity fluxes in turbulent dynamos and alpha quenching," *Phys. Rev. Letters* **93**, 205001 (2004).
- Subramanian, K. and Brandenburg, A., "Magnetic helicity density and its flux in weakly inhomogeneous turbulence," *Astrophys. J.* **648**, L71-L74 (2006).
- Vishniac, E. T. and Cho, J., "Magnetic helicity conservation and astrophysical dynamos," *Astrophys. J.* **550**, 752-760 (2001).